

Supporting Information

***Ab initio* Study for Late Steps of CO₂ and CO electroreduction: from CHCO* toward C₂ Products on Cu and CuZn Nanoclusters**

Vivianne K. Ocampo-Restrepo,* Lucas G. Verga ,* and Juarez L. F. Da Silva*

*São Carlos Institute of Chemistry, University of São Paulo, P.O. Box 780, 13560-970, São Carlos,
SP, Brazil*

E-mail: vivianne.o.restrepo@gmail.com; lucas.gverga@gmail.com; juarez_dasilva@iqsc.usp.br

Contents

1 Systems in Gas-phase: Intermediates in the Selected Paths to Ethylene, Acetaldehyde, and Ethanol Production	S-3
2 Cu₅₅ and Cu₄₂Zn₁₃ Clusters Models	S-5
2.1 Cu ₅₅ clusters	S-5
2.2 Cu ₄₂ Zn ₁₃ ICO clusters models	S-7
2.3 Comparison between the Cu ₅₅ and Cu ₄₂ Zn ₁₃ Clusters	S-9
3 Computational Tests for Adsorbed Systems	S-11
3.1 Optimization Tests to Explore Large Set of Adsorbed Structures	S-11
3.2 Tests for Vibrational Frequencies Calculations	S-16
4 Investigated Reaction Mechanisms	S-24
5 Computational Hydrogen Electrode Method	S-25
6 Gas-phase Molecules within the CHE	S-27
7 Liquid-phase Corrections	S-27
8 Solvation Contributions to the Free Energies	S-29
9 Free Energy Diagrams from CHCO to Ethanol and Ethylene	S-30
10 Projected Density of States: Intermediates on Cu₅₅ and Cu₄₂Zn₁₃	S-34
References	S-34

1 Systems in Gas-phase: Intermediates in the Selected Paths to Ethylene, Acetaldehyde, and Ethanol Production

Figure S1 displays all the species studied, while Table S1 summarizes the most important energetic and structural properties. For the C₂ species, the calculated binding energies are slightly overestimated with a maximum relative error of about 5.0 % compared to the experimental values for the following systems, namely, CH₂CO, CH₃CO, C₂H₄, CH₃CHO, CH₃CH₂O, CH₃CH₂OH. Conversely, the values for OH and H₂O are underestimated with a larger relative error of 3.00 % for the hydroxyl radical.¹

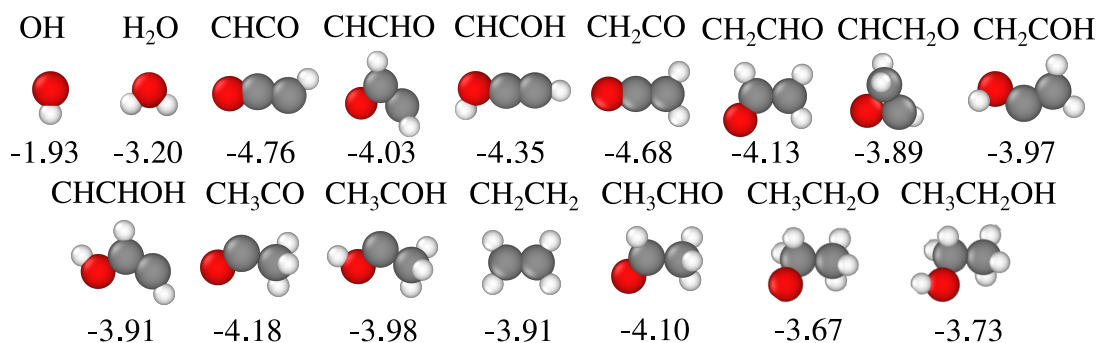


Figure S1: Species in gas-phase that participate in the reaction paths studied, where the carbon, oxygen, and hydrogen atoms are the gray, red, and white balls, respectively. The number below each species is the binding energy with $E_{\text{energy}}^{\text{ZPE}}$ correction (E_b^{ZPE}) in eV per atom.

The most stable species, more negative values for E_b , are CHCO, CHCOH, and CH₂CO, that presented the shorter bond lengths between the carbons and oxygen atoms since the central carbon is prone to keep its valence complete. Although the central carbon only binds to the other carbon and oxygen atoms, those species have differences in their OCC angle. The smaller angle for CHCO can be explained by its radical nature and the electron delocalization over the central carbon atom. While the CH₂CO and CHCOH presented OCC angle close to 180.00°, the slightly difference could be explained by a possible hybridization changes on the O atom from sp^2 to sp^3 , respectively.

Table S1: Energetic and some structural properties for all the species studied in the selected reaction paths. Absolute value for binding energy ($|E_b|$), zero point energy (E_{energy}^{ZPE}), absolute value for binding energy with E_{energy}^{ZPE} correction ($|E_b^{ZPE}|$), experimental binding energy ($E_b^{\text{Exp.}}$) at two different temperatures (T) from the literature,¹ minimum oxygen bond distance with $X = \text{H}$ or C ($d^{\text{O}-\text{X}}$), minimum carbon-carbon bond distance ($d^{\text{C}-\text{C}}$), and angle between the fragment OCC (\angle^{OCC}).

Species	$ E_b $	E_{energy}^{ZPE}	$ E_b^{ZPE} $	$E_b^{\text{Exp.}}$	$d^{\text{O}-\text{X}}$	$d^{\text{C}-\text{C}}$	\angle^{OCC}
	(eV)	(eV)	(eV)	(eV)	(Å)	(Å)	(°)
$T = 298 \text{ K}$						$T = 0 \text{ K}$	
OH	4.77	0.22	4.55	4.46	4.41	0.98	
H_2O	10.16	0.56	9.59	9.61	9.51	0.97	
CHCO	19.55	0.50	19.05			1.18	1.30 169.40
CHCHO	20.95	0.79	20.16			1.29	1.35 90.80
CHCOH	22.57	0.83	21.73			1.31	1.21 175.30
CH ₂ CO	24.22	0.83	23.39	22.45	22.24	1.17	1.31 180.00
CH ₂ CHO	25.91	1.11	24.79			1.24	1.43 123.20
CHCH ₂ O	24.50	1.16	23.34			1.37	1.45 63.30
CH ₂ COH	24.93	1.13	23.80			1.34	1.32 130.90
CHCHOH	24.56	1.11	23.45			1.39	1.31 124.20
CH ₃ CO	26.20	1.13	25.07	24.32	24.05	1.19	1.50 129.20
CH ₃ COH	27.89	1.44	26.45			1.33	1.49 107.60
C ₂ H ₄	24.81	1.35	23.47	23.35	23.07		1.33
CH ₃ CHO	30.15	1.45	28.70	28.25	27.92	1.21	1.50 124.80
CH ₃ CH ₂ O	31.06	1.68	29.38	28.88	28.50	1.35	1.53 117.30
CH ₃ CH ₂ OH	35.67	2.10	33.57	33.43	32.98	1.44	1.52 92.6

As expected, the hydrogenation on the central carbon in the CHCHO species provided the smaller OCC angle among the species with a molecular formula of C₂H₂O, a consequence of the central carbon hybridization that also impacts the binding energy, reducing the strength of their bonds compared with the other isomers. Comparing the species with the molecular formula of C₂H₃O the most stable species keep the shorter C–O bond length: CH₂CHO and CH₃CO. The remained isomers presented additional O- bonds, weakening the C–O bond and providing less stability to the species. A similar trend for the C₂H₄O species was observed, where the acetaldehyde is more stable than CH₃COH. Finally, comparing the ethylene and ethanol stability, the former presented a stronger C–C bond, typically characterized as a double bond that provides more stability for this species as evidenced by comparing the binding energy values.

2 Cu₅₅ and Cu₄₂Zn₁₃ Clusters Models

2.1 Cu₅₅ clusters

To obtain our model for the Cu₅₅ cluster, we re-optimized a set of 9 different structures from a previous study developed in our group.² Structures with high and low-symmetry were included, namely: icosahedron (ICO), cuboctahedron (CUB), disordered reduced-core (DRC), that includes models with 7 to 11 atoms in the core, tetrahedral-like models (THL), and a fragment of the FCC structure (FCCf), Figure S2. As expected, our putative global minimum configuration was the ICO structure with small differences in their properties as compared with previous results.² Then, we selected the Cu₅₅ ICO as our reference model to study the effect of the Zn in the CuZn alloy.

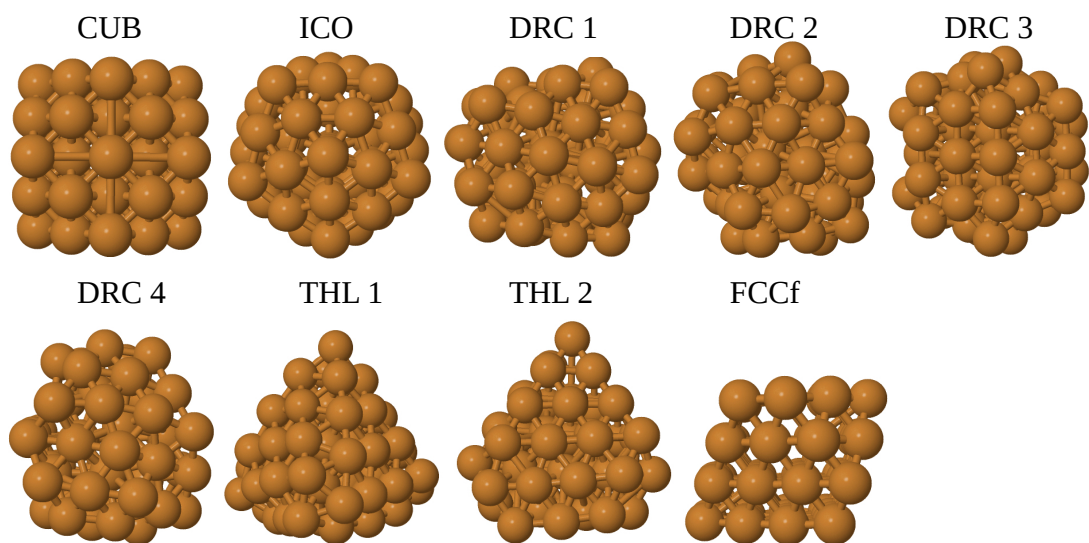


Figure S2: Structure models for the Cu₅₅ clusters.²

Table S2: Energetic, structural, and electronic properties for Cu₅₅ clusters. Relative energy (ΔE_{tot}), binding energy (E_b), highest occupied molecular orbital (HOMO), lowest unoccupied molecular orbital (LUMO), HOMO-LUMO energy gap (Gap), average effective coordination number (ECN_{av}), average interatomic distance (d_{av}), Radius (Radius), chemical order parameter (σ), and total magnetic moment (m_{tot}).

Clusters	ΔE_{tot} (eV)	E_b (eV/atom)	HOMO (eV)	LUMO (eV)	Gap (eV)	ECN _{av} (NNN)	d_{av} (Å)	Radius (Å)	σ	m_{tot} (μ_B)
PBE-light1										
THL 1	5.70	-2.79	-4.23	-4.17	0.06	7.76	2.51	6.33	1.00	1.00
THL 2	4.60	-2.81	-4.27	-4.20	0.08	7.69	2.50	6.37	1.00	1.00
DRC 4	4.20	-2.81	-4.14	-4.07	0.07	7.50	2.49	5.34	1.00	1.00
DRC 3	4.00	-2.82	-4.33	-4.26	0.07	7.57	2.49	5.30	1.00	1.00
FCCf	3.98	-2.82	-4.12	-4.05	0.06	7.84	2.50	5.88	1.00	1.00
CUB	3.60	-2.83	-4.22	-3.92	0.30	7.81	2.50	4.94	1.00	1.00
DRC 2	3.32	-2.83	-4.27	-4.19	0.07	7.66	2.50	5.36	1.00	1.00
DRC 1	3.32	-2.83	-4.25	-4.17	0.08	7.66	2.50	5.25	1.00	1.00
ICO	0.00	-2.89	-4.16	-4.12	0.04	8.38	2.52	4.81	1.00	3.00
PBE+TS-light1										
THL 1	6.57	-2.98	-4.25	-4.18	0.06	7.76	2.49	6.26	1.00	1.00
THL 2	5.33	-3.01	-4.30	-4.23	0.07	7.68	2.48	6.30	1.00	1.00
FCCf	4.87	-3.02	-4.12	-4.06	0.06	7.83	2.48	5.83	1.00	1.00
DRC 4	4.60	-3.02	-4.11	-4.05	0.07	7.53	2.47	5.33	1.00	1.00
DRC 3	4.57	-3.02	-4.36	-4.29	0.07	7.58	2.47	5.24	1.00	1.00
CUB	4.23	-3.03	-4.22	-3.93	0.29	7.82	2.48	4.90	1.00	1.00
DRC 1	3.99	-3.03	-4.36	-4.28	0.08	7.46	2.47	5.12	1.00	1.00
DRC 2	3.53	-3.04	-4.24	-4.17	0.07	7.71	2.48	5.33	1.00	1.00
ICO	0.00	-3.10	-4.16	-4.13	0.04	8.40	2.50	4.76	1.00	3.00
PBE+TS-light2										
THL 1	6.50	-3.00	-4.20	-4.13	0.07	7.76	2.49	6.25	1.00	1.00
THL 2	5.24	-3.02	-4.24	-4.17	0.07	7.68	2.48	6.30	1.00	1.00
FCCf	4.76	-3.03	-4.08	-4.01	0.07	7.83	2.48	5.82	1.00	1.00
DRC 4	4.50	-3.04	-4.07	-4.00	0.07	7.53	2.47	5.32	1.00	1.00
DRC 3	4.48	-3.04	-4.32	-4.24	0.07	7.57	2.47	5.23	1.00	1.00
CUB	4.22	-3.04	-4.17	-3.89	0.27	7.82	2.48	4.89	1.00	1.00
DRC 1	3.90	-3.05	-4.31	-4.23	0.08	7.46	2.47	5.11	1.00	1.00
DRC 2	3.46	-3.06	-4.20	-4.13	0.07	7.71	2.48	5.32	1.00	1.00
ICO	0.00	-3.12	-4.11	-4.07	0.04	8.39	2.50	4.75	1.00	3.00
PBE+TS-light3										
THL 1	6.50	-3.01	-4.23	-4.17	0.07	7.76	2.49	6.24	1.00	1.00
THL 2	5.25	-3.03	-4.28	-4.21	0.07	7.68	2.48	6.30	1.00	1.00
FCCf	4.75	-3.04	-4.11	-4.04	0.07	7.83	2.47	5.82	1.00	1.00
DRC 4	4.52	-3.05	-4.11	-4.04	0.07	7.53	2.47	5.32	1.00	1.00
DRC 3	4.49	-3.05	-4.35	-4.28	0.07	7.57	2.47	5.23	1.00	1.00
CUB	4.25	-3.05	-4.20	-3.93	0.27	7.82	2.48	4.89	1.00	1.00
DRC 1	3.91	-3.06	-4.35	-4.27	0.08	7.46	2.47	5.10	1.00	1.00
DRC 2	3.46	-3.07	-4.23	-4.16	0.07	7.71	2.48	5.32	1.00	1.00
ICO	0.00	-3.13	-4.15	-4.11	0.04	8.39	2.50	4.75	1.00	3.00

Table S3: Comparison of energetic, structural, and electronic properties for Cu₅₅^{ICO} clusters using PBE, PBE with van der Waals corrections, TS or D3 approaches, and different levels of numerical atomic orbitals wave functions, namely light 1, 2, 3, and plane-waves (PW). Binding energy (E_b), average effective coordination number (ECN_{av}), average interatomic distance (d_{av}), total magnetic moment (m_{tot}).

Cu ₅₅ ^{ICO}		E_b (eV/atom)	ECN _{av} (NNN)	d_{av} (Å)	m_{tot} (μ_B)
This study	PBE-light1	-2.89	8.38	2.52	3.00
	PBE+TS-light1	-3.10	8.40	2.50	3.00
	PBE-light2	-2.91	8.38	2.52	3.00
	PBE+TS-light2	-3.12	8.39	2.50	3.00
	PBE+TS-light3	-3.13	8.39	2.50	3.00
Literature ²	PBE-PW	-2.87	8.38	2.52	3.00
	PBE+D3-PW	-3.12	8.40	2.49	3.00

2.2 Cu₄₂Zn₁₃ ICO clusters models

The 55-atom gas-phase Cu cluster in the icosahedron structure was selected as our cluster reference to evaluate the effect of Zn in the CO₂ reduction on Cu-rich CuZn alloys. To perform a comparison among the results isolating the structural effects, we use the icosahedron model to construct the Cu₄₂Zn₁₃ alloy. This composition leads to a Cu/Zn ratio of 3.2, which is close to the experimental ratio reported to increase the ethylene and ethanol production.^{3,4} We explore different cluster models, considering core-shell types structures with most Zn atoms at the core ($C_{Zn}S_{Cu}$), with most of the Zn at the shell ($C_{Cu}S_{Zn}$), and a segregated cluster (Seg_{Cu-Zn}).

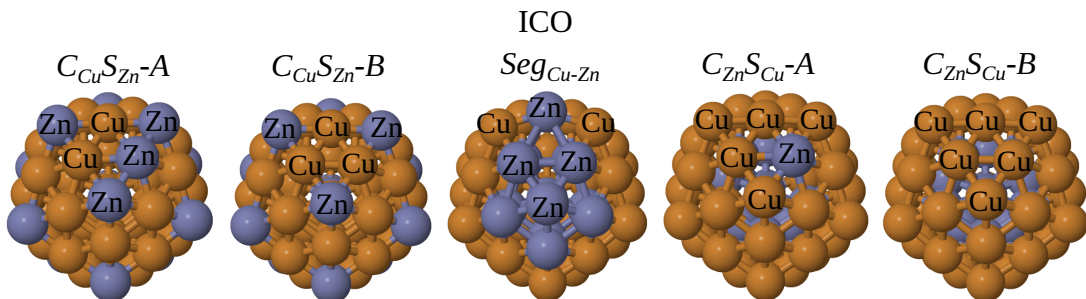


Figure S3: Cu₄₂Zn₁₃ ICO clusters models. Core-shell type core Cu-rich, $C_{Cu}S_{Zn}$; core-shell type core Zn-rich, $C_{Zn}S_{Cu}$; and segregated cluster, Seg_{Cu-Zn} .

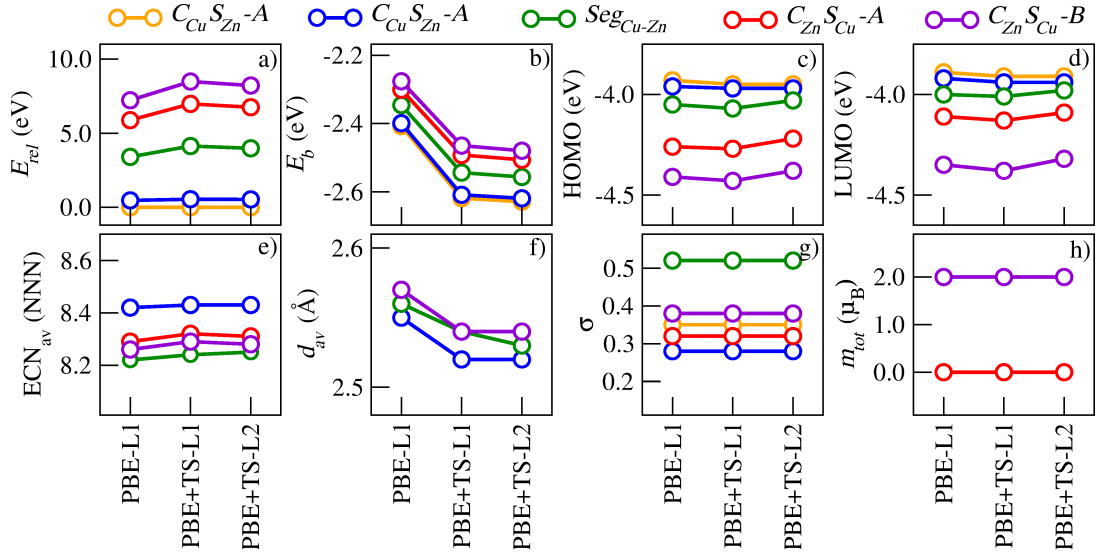


Figure S4: Properties of the $\text{Cu}_{42}\text{Zn}_{13}$ ICO clusters as a function of basis function and functionals.

Table S4: Energetic, structural, and electronic properties for $\text{Cu}_{42}\text{Zn}_{13}$ ICO clusters. Relative energy, ΔE_{tot} ; Binding energy, E_b ; highest occupied molecular orbital, HOMO; lowest unoccupied molecular orbital, LUMO; HOMO-LUMO gap, Gap; average effective coordination number, ECN_{av} ; average interatomic distance, d_{av} ; Radius, Radius; chemical order parameter, σ ; total magnetic moment, m_{tot} .

Clusters	ΔE_{tot} (eV)	E_b (eV/atom)	HOMO (eV)	LUMO (eV)	Gap (eV)	ECN_{av} (NNN)	d_{av} (Å)	Radius (Å)	σ	m_{tot} (μ_B)
PBE-light1										
$C_{\text{Zn}}S_{\text{Cu}} - B$	7.22	-2.28	-4.41	-4.35	0.06	8.26	2.57	4.93	0.38	2.00
$C_{\text{Zn}}S_{\text{Cu}} - A$	5.88	-2.30	-4.26	-4.11	0.15	8.29	2.57	4.92	0.32	0.00
$Seg_{\text{Cu-Zn}}$	3.40	-2.35	-4.05	-4.00	0.05	8.22	2.56	4.96	0.52	2.00
$C_{\text{Cu}}S_{\text{Zn}} - B$	0.46	-2.40	-3.96	-3.92	0.04	8.42	2.55	4.87	0.28	2.00
$C_{\text{Cu}}S_{\text{Zn}} - A$	0.00	-2.41	-3.93	-3.89	0.04	8.42	2.55	4.88	0.35	2.00
PBE+TS-light1										
$C_{\text{Zn}}S_{\text{Cu}} - B$	8.48	-2.46	-4.43	-4.38	0.05	8.29	2.54	4.87	0.38	2.00
$C_{\text{Zn}}S_{\text{Cu}} - A$	6.97	-2.49	-4.27	-4.13	0.14	8.32	2.54	4.87	0.32	0.00
$Seg_{\text{Cu-Zn}}$	4.13	-2.54	-4.07	-4.01	0.05	8.24	2.54	4.91	0.52	2.00
$C_{\text{Cu}}S_{\text{Zn}} - B$	0.55	-2.61	-3.97	-3.94	0.04	8.43	2.52	4.82	0.28	2.00
$C_{\text{Cu}}S_{\text{Zn}} - A$	0.00	-2.62	-3.95	-3.91	0.04	8.43	2.52	4.82	0.35	2.00
PBE+TS-light2										
$C_{\text{Zn}}S_{\text{Cu}} - B$	8.21	-2.48	-4.38	-4.32	0.05	8.28	2.54	4.87	0.38	2.00
$C_{\text{Zn}}S_{\text{Cu}} - A$	6.75	-2.51	-4.22	-4.09	0.13	8.31	2.54	4.87	0.32	0.00
$Seg_{\text{Cu-Zn}}$	3.98	-2.56	-4.03	-3.98	0.05	8.25	2.53	4.91	0.52	2.00
$C_{\text{Cu}}S_{\text{Zn}} - B$	0.53	-2.62	-3.97	-3.94	0.04	8.43	2.52	4.82	0.28	2.00
$C_{\text{Cu}}S_{\text{Zn}} - A$	0.00	-2.63	-3.95	-3.91	0.04	8.43	2.52	4.82	0.35	2.00

2.3 Comparison between the Cu₅₅ and Cu₄₂Zn₁₃ Clusters

Table S5 contains data related to energetic, structural, and electronic properties. About the structural properties, the Cu₄₂Zn₁₃ cluster presented small differences compared with the Cu₅₅, e.g., larger radius and d_{av} values. It is a consequence of the larger Zn–Zn and Cu–Zn bond lengths, compared to Cu₅₅ cluster, that deviates the average value of the bond distances. Contrary, the binding energy is more affected, where the alloy requires less energy to be atomized.

Table S5: Comparison of energetic, structural, and electronic properties for Cu₅₅ and Cu₄₂Zn₁₃ clusters. Binding energy per atom (E_b); highest occupied molecular orbital (HOMO); lowest unoccupied molecular orbital (LUMO); HOMO-LUMO gap (Gap); average effective coordination number (ECN_{av}); average interatomic distance (d_{av}); Radius (Radius); charge at shell surface (q_S); and total magnetic moment (m_{tot}).

Clusters	E_b (eV/atom)	HOMO (eV)	LUMO (eV)	Gap (eV)	ECN _{av} (NNN)	d_{av} (Å)	Radius (Å)	q_S (e)	m_{tot} (μ_B)
Cu ₅₅	-3.12	-4.11	-4.07	0.04	8.39	2.50	4.75	-0.19	3.00
Cu ₄₂ Zn ₁₃	-2.63	-3.95	-3.91	0.04	8.43	2.52	4.82	-0.14	2.00

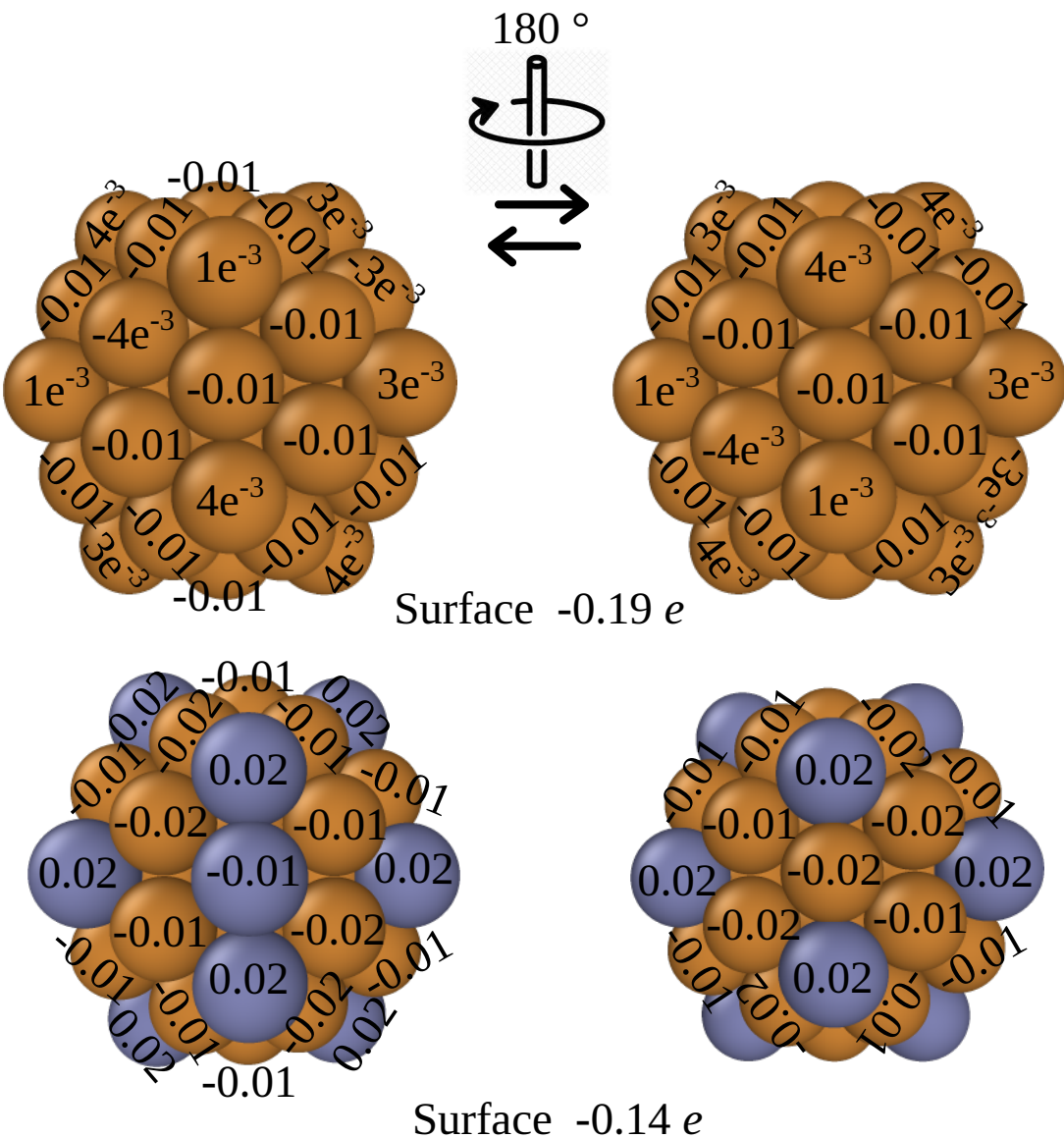


Figure S5: Hirshfeld charge analysis for Cu₅₅ and Cu₄₂Zn₁₃ Clusters.

Regarding electronic properties, the magnetic moment is reduced by the introduction of the Zn while the HOMO-LUMO gap keeps unaltered. However, the HOMO and LUMO energies suffer small shifts induced by the Zn. Finally, we analyzed the charge at the cluster surface, observing that the alloy presented a less negative net charge at the surface compared to the Cu₅₅ cluster. It could be an effect induced by the electronegativity differences, where the Cu tends to accumulate charge while the Zn tends to donate it when they are together.

3 Computational Tests for Adsorbed Systems

3.1 Optimization Tests to Explore Large Set of Adsorbed Structures

Below are the results comparing the set of parameters for the scanning, A, and the set to get the final data, B.

Set of parameters A:

basis set: light1

vdw_correction_hirshfeld:off

sc_accuracy_etot 1.0E – 4

sc_accuracy_rho 1.0E – 3

sc_accuracy_eev 1.0E – 1

sc_accuracy_forces 1.0E – 2

Relaxation: *relax_geometrytrm* 1.0E – 1

Set of parameters B:

basis set: light2;

vdw_correction_hirshfeld:on

sc_accuracy_etot 1.0E – 5

sc_accuracy_rho 1.0E – 4

sc_accuracy_eev 1.0E – 2

sc_accuracy_forces 1.0E – 3

Relaxation: *relax_geometrytrm* 1.0E – 2

Tables S6 – 9 and the Figure S6 compare the data for CHCO and CHCHO on Cu₅₅ and Cu₄₂Zn₁₃ clusters. The scanning considered about 20 – 30 structures for CHCO and CHCHO. To reduce the set of structures for the calculation with set B, we performed a k-means analysis, including the energetic information gathered from the calculations with set A. Figure S9 at the top shows the relative energy from set B *versus* set A. The relative energy calculation employed the lowest energy structure provided from set B as the reference. Figure S9 at the bottom shows the relative energy difference between sets B and A for each configuration. Also, orange symbols and X green highlight the lowest energy structure obtained via set A and B, respectively. The

main difference was for CHCO on Cu₅₅, where the higher energy structure predicted from set A becomes the lowest one when used the set B. We observed structures from set A provided the same minimum when optimized with set B, as informed by similarity in their properties, Table S6. For the remaining systems, both sets predicted the same lowest energy structures. Then, we used the predicted lowest energy structures with set A and refined them with set B to obtain the final data.

Table S6: Comparison between set of parameters A and B for CHCO adsorbed on Cu₅₅ cluster. Relative energy, ΔE_{tot} ; adsorption energy, E_{ad} ; highest occupied molecular orbital, HOMO; lowest unoccupied molecular orbital, LUMO; HOMO-LUMO gap, Gap; minimum bond distance of C to Cu₅₅, d^{C-Cu} ; minimum bond distance of O to Cu₅₅, d^{O-Cu} ; minimum bond distance of H to Cu₅₅, d^{H-Cu} ; total magnetic moment, m_{tot} .

Structures	ΔE_{tot} (eV)	E_{ad} (eV)	HOMO (eV)	LUMO (eV)	Gap (eV)	d^{C-Cu} (Å)	d^{O-Cu} (Å)	d^{H-Cu} (Å)	m_{tot} (μ_B)
CHCO/Cu ₅₅									
Set A									
4	0.00		-4.33	-4.29	0.04	1.91	3.69	2.66	2
9	-0.03		-4.23	-4.19	0.04	1.97	2.10	2.81	2
10	-0.03		-4.25	-4.19	0.06	1.97	2.09	2.82	2
20	-0.13		-4.24	-4.13	0.11	1.96	2.15	2.76	0
3	-0.45		-4.19	-4.11	0.08	2.06	3.37	2.57	0
18	-0.45		-4.19	-4.11	0.08	2.06	3.41	2.48	0
23	-0.57		-4.23	-4.17	0.06	2.02	3.51	2.70	2
5	-0.57		-4.22	-4.17	0.05	2.02	3.61	2.70	0
12	-0.58		-4.22	-4.18	0.04	2.03	3.69	2.70	0
19	-0.59		-4.23	-4.16	0.06	2.03	3.69	2.70	2
Set B									
10	0.58	-2.22	-4.20	-4.15	0.06	1.97	2.08	2.82	2
9	0.57	-2.22	-4.20	-4.15	0.06	1.97	2.08	2.82	2
20	0.46	-2.33	-4.20	-4.10	0.10	1.96	2.13	2.76	0
18	0.09	-2.70	-4.14	-4.06	0.08	2.09	3.44	2.20	0
3	0.09	-2.71	-4.14	-4.06	0.08	2.09	3.43	2.20	0
12	0.02	-2.77	-4.17	-4.14	0.03	2.02	3.65	2.70	0
5	0.02	-2.77	-4.17	-4.14	0.03	2.02	3.66	2.70	0
19	0.00	-2.79	-4.18	-4.12	0.06	2.03	3.65	2.71	2
23	0.00	-2.79	-4.18	-4.12	0.06	2.03	3.66	2.71	2
4	0.00	-2.79	-4.18	-4.12	0.06	2.03	3.67	2.70	2

Table S7: Comparison between set of parameters A and B for CHCHO adsorbed on Cu₅₅ cluster. Relative energy, ΔE_{tot} ; adsorption energy, E_{ad} ; highest occupied molecular orbital, HOMO; lowest unoccupied molecular orbital, LUMO; HOMO-LUMO gap, Gap; minimum bond distance of C to Cu₅₅, d^{C-Cu} ; minimum bond distance of O to Cu₅₅, d^{O-Cu} ; minimum bond distance of H to Cu₅₅, d^{H-Cu} ; total magnetic moment, m_{tot} .

Structures	ΔE_{tot} (eV)	E_{ad} (eV)	HOMO (eV)	LUMO (eV)	Gap (eV)	d^{C-Cu} (Å)	d^{O-Cu} (Å)	d^{H-Cu} (Å)	m_{tot} (μ_B)
CHCHO/Cu ₅₅									
Set A									
1	3.04		-4.27	-4.22	0.04	2.93	1.97	2.95	1
22	2.76		-4.26	-4.20	0.06	2.95	2.00	3.12	3
3	0.81		-4.33	-4.27	0.06	1.96	3.86	1.93	1
20	0.81		-4.32	-4.26	0.06	1.96	3.86	1.89	1
13	0.73		-4.36	-4.30	0.05	1.98	3.76	1.82	1
23	0.21		-4.17	-4.11	0.06	2.01	2.01	2.65	1
9	0.05		-4.23	-4.16	0.07	1.97	1.95	2.63	1
10	0.01		-4.23	-4.18	0.06	2.00	1.93	2.66	1
15	0.00		-4.23	-4.18	0.05	2.00	1.94	2.67	1
6	-0.01		-4.23	-4.18	0.06	2.00	1.94	2.67	1
Set B									
22	3.10	-1.12	-4.24	-4.19	0.05	2.97	1.97	3.13	1
1	3.10	-1.12	-4.24	-4.19	0.05	2.93	1.97	2.89	1
3	0.79	-3.43	-4.28	-4.22	0.06	1.95	3.79	1.83	1
20	0.79	-3.43	-4.28	-4.22	0.06	1.95	3.78	1.83	1
13	0.70	-3.52	-4.32	-4.26	0.06	1.98	3.68	1.77	1
23	0.16	-4.06	-4.11	-4.05	0.06	1.98	2.00	2.66	1
9	0.05	-4.17	-4.19	-4.12	0.07	1.98	1.94	2.64	1
10	0.00	-4.22	-4.19	-4.14	0.06	2.00	1.94	2.68	1
6	0.00	-4.22	-4.19	-4.14	0.06	2.00	1.94	2.68	1
15	0.00	-4.22	-4.19	-4.14	0.06	2.00	1.94	2.68	1

Table S8: Comparison between set of parameters A and B for CHCO adsorbed on Cu₄₂Zn₁₃ cluster. Relative energy, ΔE_{tot} ; adsorption energy, E_{ad} ; highest occupied molecular orbital, HOMO; lowest unoccupied molecular orbital, LUMO; HOMO-LUMO gap, Gap; minimum bond distance of C to Cu₄₂Zn₁₃, $d^{C-Cu_{42}Zn_{13}}$; minimum bond distance of O to Cu₄₂Zn₁₃, $d^{O-Cu_{42}Zn_{13}}$; minimum bond distance of H to Cu₄₂Zn₁₃, $d^{H-Cu_{42}Zn_{13}}$; total magnetic moment, m_{tot} .

Structures	ΔE_{tot} (eV)	E_{ad} (eV)	HOMO (eV)	LUMO (eV)	Gap (eV)	$d^{C-Cu_{42}Zn_{13}}$ (Å)	$d^{O-Cu_{42}Zn_{13}}$ (Å)	$d^{H-Cu_{42}Zn_{13}}$ (Å)	m_{tot} (μ_B)
CHCO/Cu ₄₂ Zn ₁₃									
Set A									
15	1.39	-4.16	-4.10	0.06	2.88	1.89	5.03	1	
2	0.66	-3.96	-3.91	0.05	2.05	2.19	2.82	1	
22	0.60	-4.02	-3.97	0.05	1.99	3.70	2.73	1	
1	0.41	-3.97	-3.90	0.07	2.10	3.50	2.79	1	
19	0.41	-3.97	-3.91	0.07	2.10	3.29	2.76	1	
29	0.39	-3.96	-3.92	0.04	2.01	2.41	2.80	1	
13	0.26	-3.98	-3.93	0.05	2.03	2.16	2.84	1	
23	0.22	-4.05	-3.99	0.06	1.95	3.70	2.74	1	
20	0.22	-4.09	-4.02	0.07	1.95	3.74	2.69	1	
7	0.07	-3.94	-3.91	0.04	2.09	3.71	2.70	1	
3	0.03	-3.97	-3.90	0.07	2.11	3.55	2.78	1	
27	0.03	-3.96	-3.90	0.06	2.10	3.68	2.79	1	
8	0.03	-3.98	-3.91	0.07	2.10	3.79	2.75	1	
16	0.02	-3.99	-3.92	0.07	2.10	3.79	2.75	1	
21	0.00	-3.97	-3.91	0.05	2.10	3.76	2.74	1	
Set B									
29	0.44	-2.78	-3.96	-3.92	0.04	2.01	2.30	2.81	1
19	0.40	-2.81	-3.98	-3.92	0.06	2.09	3.31	2.78	1
1	0.38	-2.84	-3.98	-3.91	0.07	2.09	3.38	2.78	1
15	0.37	-2.85	-4.01	-3.96	0.05	2.00	2.09	2.78	1
20	0.31	-2.91	-4.10	-4.02	0.07	1.94	3.71	2.68	1
13	0.30	-2.92	-3.99	-3.94	0.05	2.01	2.17	2.83	1
23	0.29	-2.93	-4.08	-4.01	0.07	1.94	3.72	2.68	1
22	0.21	-3.01	-3.93	-3.89	0.03	2.12	3.78	2.79	1
2	0.21	-3.01	-3.93	-3.89	0.03	2.12	3.79	2.79	1
7	0.04	-3.18	-3.95	-3.92	0.03	2.08	3.72	2.75	1
8	0.04	-3.18	-3.99	-3.92	0.07	2.09	3.72	2.76	1
27	0.02	-3.20	-3.98	-3.92	0.06	2.08	3.72	2.75	1
16	0.02	-3.20	-4.00	-3.93	0.07	2.08	3.71	2.75	1
3	0.01	-3.20	-3.99	-3.92	0.07	2.09	3.70	2.76	1
21	0.00	-3.22	-3.98	-3.93	0.05	2.09	3.72	2.74	1

Table S9: Comparison between set of parameters A and B CHCHO adsorbed on Cu₄₂Zn₁₃ cluster. Relative energy, ΔE_{tot} ; adsorption energy, E_{ad} ; highest occupied molecular orbital, HOMO; lowest unoccupied molecular orbital, LUMO; HOMO-LUMO gap, Gap; minimum bond distance of C to Cu₄₂Zn₁₃, $d^{C-Cu_{42}Zn_{13}}$; minimum bond distance of O to Cu₄₂Zn₁₃, $d^{O-Cu_{42}Zn_{13}}$; minimum bond distance of H to Cu₄₂Zn₁₃, $d^{H-Cu_{42}Zn_{13}}$; total magnetic moment, m_{tot} .

Structures	ΔE_{tot} (eV)	E_{ad} (eV)	HOMO (eV)	LUMO (eV)	Gap (eV)	$d^{C-Cu_{42}Zn_{13}}$ (Å)	$d^{O-Cu_{42}Zn_{13}}$ (Å)	$d^{H-Cu_{42}Zn_{13}}$ (Å)	m_{tot} (μ_B)
CHCHO/Cu ₄₂ Zn ₁₃									
Set A									
12	2.83	-4.12	-4.06	0.06	2.85	1.86	3.00	2	
15	2.79	-3.95	-3.90	0.05	3.06	2.03	3.35	2	
4	1.67	-4.16	-4.03	0.13	1.93	1.94	2.63	0	
14	1.27	-4.05	-3.95	0.10	2.05	2.06	1.79	0	
1	1.11	-4.13	-4.04	0.08	2.03	3.87	2.25	0	
19	1.06	-4.02	-3.94	0.08	2.00	2.44	1.70	0	
3	0.93	-4.15	-4.08	0.07	2.00	3.85	1.86	0	
24	0.85	-4.14	-4.03	0.11	2.01	3.77	1.80	0	
18	0.84	-4.16	-4.06	0.10	2.01	3.86	1.84	0	
23	0.57	-3.97	-3.89	0.08	2.05	2.05	2.74	0	
28	0.50	-4.13	-4.02	0.11	1.91	1.89	2.60	0	
11	0.37	-4.00	-3.95	0.05	2.04	1.97	2.74	0	
16	0.09	-4.02	-3.96	0.06	2.05	1.96	2.73	0	
27	0.02	-4.00	-3.90	0.11	2.06	1.96	2.76	0	
8	0.00	-4.00	-3.91	0.09	2.07	1.94	2.71	0	
Set B									
14	1.19	-3.63	-4.06	-3.96	0.10	2.04	2.05	1.78	0
1	1.03	-3.79	-4.13	-4.05	0.08	2.03	3.92	2.01	0
19	0.96	-3.86	-4.02	-3.94	0.08	2.02	2.26	1.70	0
12	0.95	-3.87	-4.07	-3.97	0.10	2.00	2.08	1.74	0
3	0.90	-3.92	-4.16	-4.09	0.06	2.01	3.76	1.79	0
24	0.83	-3.99	-4.15	-4.04	0.11	2.01	3.75	1.78	0
18	0.82	-4.00	-4.17	-4.07	0.10	2.00	3.76	1.78	0
28	0.49	-4.34	-4.14	-4.03	0.11	1.91	1.89	2.60	0
15	0.43	-4.39	-4.13	-3.99	0.13	1.94	1.89	2.65	0
11	0.33	-4.50	-4.00	-3.97	0.03	2.04	1.97	2.73	0
16	0.07	-4.75	-4.04	-3.98	0.06	2.03	1.95	2.72	0
27	0.03	-4.80	-4.02	-3.91	0.11	2.06	1.95	2.75	0
23	0.02	-4.80	-4.02	-3.91	0.11	2.06	1.95	2.75	0
4	0.00	-4.82	-4.02	-3.92	0.10	2.03	1.96	2.72	0
8	0.00	-4.82	-4.02	-3.92	0.09	2.07	1.93	2.71	0

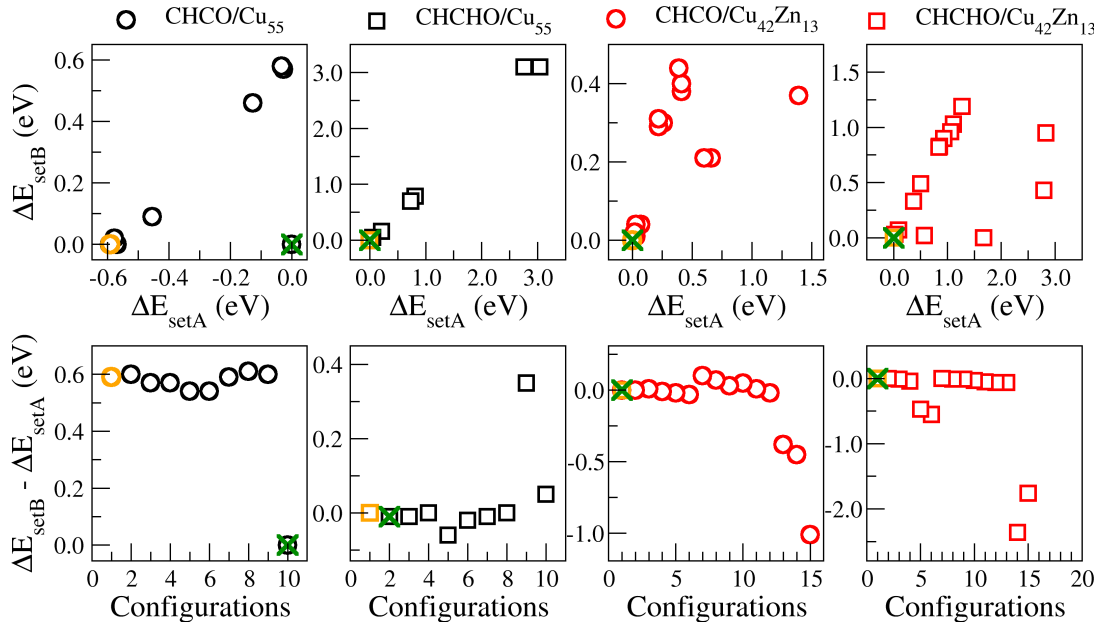


Figure S6: Comparison between set of parameters A and B for CHCO and CHCHO adsorbed on Cu₅₅ and Cu₄₂Zn₁₃. Orange symbols and X green highlight the lowest energy structure obtained by set A and B, respectively.

3.2 Tests for Vibrational Frequencies Calculations

Table S10: Vibrational frequencies results for CHCO on Cu₅₅ computing the frequencies of the normal modes by relaxing all atoms and the frequencies related to CHCO species by fixing the Cu₅₅ atoms. We included the values for zero-point energy (E_{energy}^{ZPE}) contributions of each normal mode, and the last row informs the sum of E_{energy}^{ZPE} using only the information related to the CHCO normal modes.

Normal modes	All atoms relaxed	E_{energy}^{ZPE}	CHCO on Cu _{55fixed}	E_{energy}^{ZPE}
1	-0.72	0.00		
2	-0.34	0.00		
3	-0.02	0.00		
4	0.00	0.00		
5	0.00	0.00		
6	0.22	0.00		
7	32.51	0.00	35.16	0.00
8	37.59	0.00	43.89	0.00

Continued on next page

Table S10: Vibrational frequencies results for CHCO on Cu₅₅ computing the frequencies of the normal modes by relaxing all atoms and the frequencies related to CHCO species by fixing the Cu₅₅ atoms. We included the values for zero-point energy (E_{energy}^{ZPE}) contributions of each normal mode, and the last row informs the sum of E_{energy}^{ZPE} using only the information related to the CHCO normal modes.

Normal modes	All atoms relaxed	E_{energy}^{ZPE}	CHCO on Cu₅₅fixed	E_{energy}^{ZPE}
9	58.12	0.00		
10	61.20	0.00		
11	62.73	0.00		
12	62.97	0.00		
13	64.05	0.00		
14	66.45	0.00		
15	67.62	0.00		
16	70.42	0.00		
17	74.83	0.00		
18	76.33	0.00		
19	77.44	0.00		
20	80.34	0.00		
21	81.96	0.01		
22	85.64	0.01		
23	86.00	0.01		
24	86.95	0.01		
25	88.41	0.01		
26	89.32	0.01		
27	90.18	0.01		
28	91.55	0.01		
29	91.86	0.01		
30	92.55	0.01		

Continued on next page

Table S10: Vibrational frequencies results for CHCO on Cu₅₅ computing the frequencies of the normal modes by relaxing all atoms and the frequencies related to CHCO species by fixing the Cu₅₅ atoms. We included the values for zero-point energy (E_{energy}^{ZPE}) contributions of each normal mode, and the last row informs the sum of E_{energy}^{ZPE} using only the information related to the CHCO normal modes.

Normal modes	All atoms relaxed	E_{energy}^{ZPE}	CHCO on Cu₅₅fixed	E_{energy}^{ZPE}
31	93.92	0.01		
32	94.49	0.01		
33	95.49	0.01		
34	95.83	0.01		
35	96.23	0.01		
36	97.48	0.01		
37	97.94	0.01		
38	99.01	0.01		
39	100.31	0.01		
40	100.42	0.01		
41	102.21	0.01		
42	103.59	0.01		
43	104.26	0.01	107.38	0.01
44	108.14	0.01		
45	109.96	0.01		
46	110.56	0.01		
47	110.92	0.01		
48	111.90	0.01		
49	113.92	0.01		
50	114.52	0.01		
51	115.61	0.01		
52	116.08	0.01		

Continued on next page

Table S10: Vibrational frequencies results for CHCO on Cu₅₅ computing the frequencies of the normal modes by relaxing all atoms and the frequencies related to CHCO species by fixing the Cu₅₅ atoms. We included the values for zero-point energy (E_{energy}^{ZPE}) contributions of each normal mode, and the last row informs the sum of E_{energy}^{ZPE} using only the information related to the CHCO normal modes.

Normal modes	All atoms relaxed	E_{energy}^{ZPE}	CHCO on Cu₅₅fixed	E_{energy}^{ZPE}
53	117.25	0.01		
54	117.61	0.01		
55	118.46	0.01		
56	118.74	0.01		
57	119.18	0.01		
58	119.43	0.01		
59	120.07	0.01		
60	120.64	0.01		
61	121.95	0.01		
62	122.04	0.01		
63	122.89	0.01		
64	123.28	0.01		
65	124.51	0.01		
66	125.18	0.01		
67	125.61	0.01		
68	125.85	0.01		
69	127.02	0.01		
70	127.58	0.01		
71	129.67	0.01		
72	130.67	0.01		
73	131.68	0.01		
74	134.33	0.01		
<hr/>				

Continued on next page

Table S10: Vibrational frequencies results for CHCO on Cu₅₅ computing the frequencies of the normal modes by relaxing all atoms and the frequencies related to CHCO species by fixing the Cu₅₅ atoms. We included the values for zero-point energy (E_{energy}^{ZPE}) contributions of each normal mode, and the last row informs the sum of E_{energy}^{ZPE} using only the information related to the CHCO normal modes.

Normal modes	All atoms relaxed	E_{energy}^{ZPE}	CHCO on Cu₅₅fixed	E_{energy}^{ZPE}
75	135.36	0.01		
76	135.69	0.01		
77	136.44	0.01		
78	136.74	0.01		
79	139.07	0.01		
80	139.81	0.01		
81	142.55	0.01		
82	144.20	0.01		
83	144.62	0.01		
84	148.71	0.01		
85	149.30	0.01		
86	150.19	0.01		
87	152.01	0.01		
88	153.52	0.01		
89	154.54	0.01		
90	155.72	0.01		
91	155.93	0.01		
92	156.53	0.01		
93	156.78	0.01		
94	157.34	0.01		
95	158.42	0.01		
96	158.73	0.01		

Continued on next page

Table S10: Vibrational frequencies results for CHCO on Cu₅₅ computing the frequencies of the normal modes by relaxing all atoms and the frequencies related to CHCO species by fixing the Cu₅₅ atoms. We included the values for zero-point energy (E_{energy}^{ZPE}) contributions of each normal mode, and the last row informs the sum of E_{energy}^{ZPE} using only the information related to the CHCO normal modes.

Normal modes	All atoms relaxed	E_{energy}^{ZPE}	CHCO on Cu₅₅fixed	E_{energy}^{ZPE}
97	159.76	0.01		
98	160.28	0.01		
99	162.50	0.01		
100	163.07	0.01		
101	164.13	0.01		
102	164.31	0.01		
103	165.78	0.01		
104	165.87	0.01		
105	166.70	0.01		
106	167.48	0.01		
107	168.28	0.01		
108	168.46	0.01		
109	168.93	0.01		
110	170.07	0.01		
111	170.33	0.01		
112	170.39	0.01		
113	171.91	0.01		
114	173.22	0.01		
115	173.63	0.01		
116	174.95	0.01		
117	179.22	0.01		
118	180.23	0.01		

Continued on next page

Table S10: Vibrational frequencies results for CHCO on Cu₅₅ computing the frequencies of the normal modes by relaxing all atoms and the frequencies related to CHCO species by fixing the Cu₅₅ atoms. We included the values for zero-point energy (E_{energy}^{ZPE}) contributions of each normal mode, and the last row informs the sum of E_{energy}^{ZPE} using only the information related to the CHCO normal modes.

Normal modes	All atoms relaxed	E_{energy}^{ZPE}	CHCO on Cu₅₅fixed	E_{energy}^{ZPE}
119	180.48	0.01		
120	181.34	0.01		
121	182.18	0.01		
122	184.41	0.01		
123	185.93	0.01		
124	186.09	0.01		
125	188.80	0.01		
126	190.33	0.01		
127	191.79	0.01		
128	192.68	0.01		
129	194.98	0.01		
130	204.12	0.01		
131	208.13	0.01		
132	208.39	0.01		
133	209.96	0.01		
134	211.62	0.01		
135	213.37	0.01		
136	214.13	0.01		
137	214.83	0.01		
138	215.28	0.01		
139	216.38	0.01		
140	216.53	0.01		

Continued on next page

Table S10: Vibrational frequencies results for CHCO on Cu₅₅ computing the frequencies of the normal modes by relaxing all atoms and the frequencies related to CHCO species by fixing the Cu₅₅ atoms. We included the values for zero-point energy (E_{energy}^{ZPE}) contributions of each normal mode, and the last row informs the sum of E_{energy}^{ZPE} using only the information related to the CHCO normal modes.

Normal modes	All atoms relaxed	E_{energy}^{ZPE}	CHCO on Cu₅₅fixed	E_{energy}^{ZPE}
141	217.58	0.01		
142	218.12	0.01		
143	219.17	0.01		
144	219.87	0.01		
145	229.73	0.01		
146	231.64	0.01		
147	232.05	0.01		
148	233.50	0.01		
149	234.31	0.01		
150	234.67	0.01		
151	235.23	0.01		
152	236.21	0.01		
153	243.65	0.02		
154	245.25	0.02		
155	245.37	0.02		
156	248.26	0.02		
157	265.46	0.02	249.87	0.02
158	272.12	0.02		
159	272.88	0.02		
160	274.29	0.02		
161	275.07	0.02		
162	276.40	0.02		

Continued on next page

Table S10: Vibrational frequencies results for CHCO on Cu₅₅ computing the frequencies of the normal modes by relaxing all atoms and the frequencies related to CHCO species by fixing the Cu₅₅ atoms. We included the values for zero-point energy (E_{energy}^{ZPE}) contributions of each normal mode, and the last row informs the sum of E_{energy}^{ZPE} using only the information related to the CHCO normal modes.

Normal modes	All atoms relaxed	E_{energy}^{ZPE}	CHCO on Cu₅₅fixed	E_{energy}^{ZPE}
163	277.82	0.02		
164	278.64	0.02		
165	290.52	0.02		
166	298.97	0.02		
167	326.25	0.02		
168	328.02	0.02		
169	328.46	0.02		
170	379.97	0.02	350.88	0.02
171	522.31	0.03	521.70	0.03
172	562.30	0.03	558.26	0.03
173	576.21	0.04	575.02	0.04
174	954.79	0.06	954.70	0.06
175	1170.66	0.07	1170.59	0.07
176	2085.53	0.13	2085.51	0.13
177	3120.18	0.19	3120.07	0.19
ΣE_{energy}^{ZPE} of CHCO		0.60		0.60

4 Investigated Reaction Mechanisms

Herein, we explored all the proton-coupled electron transfer (PCET) steps from CHCO until ethylene, acetaldehyde, and ethanol as illustrated in Figure S7.

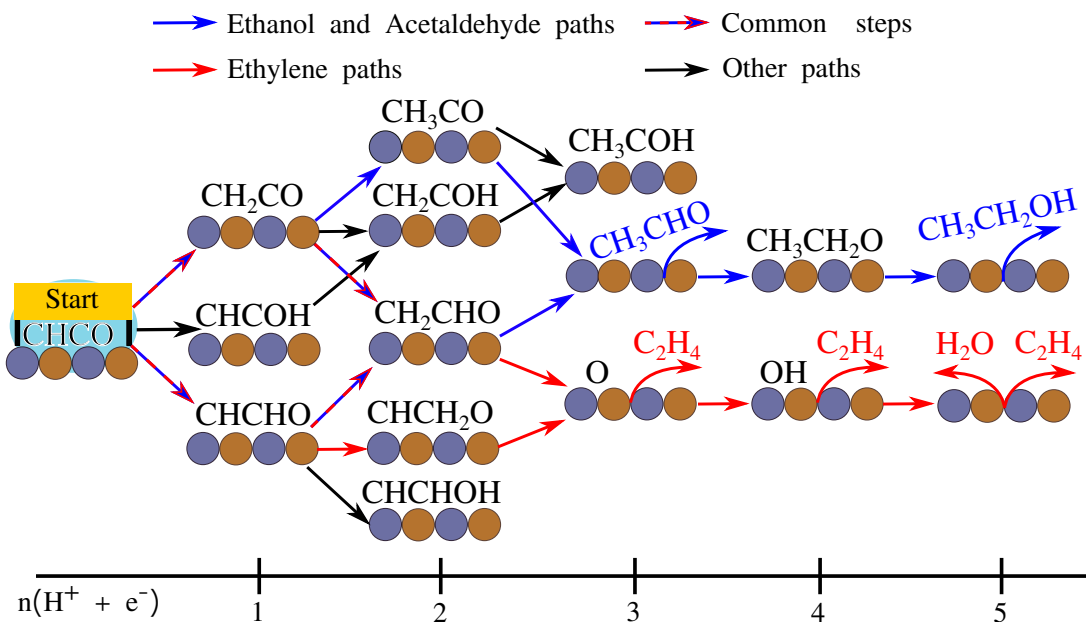


Figure S7: Possible reaction pathways via proton-coupled electron transfer steps after $\text{CH}-\text{CO}$ coupling for CO2RR or CORR toward ethylene, acetaldehyde, and ethanol production. The final products are highlighted in blue for ethanol and acetaldehyde and red for ethylene and water.

5 Computational Hydrogen Electrode Method

To study the series of proton-coupled electron transfer steps of the reaction pathways into ethanol and ethylene (shown in Figure S7), we employed the computational hydrogen electrode (CHE) model.^{5,6} In the CHE method, each elementary step within a given reaction pathway involved the addition of a proton and an electron, $\text{H}^+ + e^-$. We can relate the chemical potential of the $\text{H}^+ + e^-$ with the $\frac{1}{2}\text{H}_2$ by setting the reference potential to be that of the standard hydrogen electrode (SHE), which is defined at pH 0. Then, the products and reactants of the following equation are in equilibrium:



The equilibrium in equation (1) at electrode potential $U = 0$ versus SHE allows the following equality:

$$\Delta G_{\frac{1}{2}\text{H}_2 \rightleftharpoons \text{H}^+ + e^-} = (\mu'_{\text{H}^+} + \mu'_{e^-}) - \frac{1}{2}\mu_{\text{H}_2} = 0, \quad (2)$$

where μ' is the electrochemical potential and μ the chemical potential. From equation (2) the

Gibbs free energy for $\frac{1}{2}\text{H}_2$ is equal to the Gibbs free energy of $\text{H}^+ + \text{e}^-$: $\frac{1}{2}G_{\text{H}_2} = G_{\text{H}^+ + \text{e}^-}$. An additional contribution is the influence of applied electrical potential that is included by setting the total energy of the electron in the electrode as $-qU$ where q is the elementary charge. Thus, the free energy of each step will vary with U according to $\Delta G(U) = \Delta G(U=0) - eU$. Therefore, changes in the electrode potential can be adjusted by changing the energy by $-eU$.

For evaluating the Gibbs free energy change of the elementary steps, the Gibbs free energy for each component involving an adsorbed species was computed by:

$$G^{\text{ads/TM}_{55}} = E_{\text{tot}}^{\text{ads/TM}_{55}} + E_{\text{energy}}^{\text{ZPE}} + \int C_p dT - TS + E_{\text{sol}}, \quad (3)$$

where $E_{\text{tot}}^{\text{ads/TM}_{55}}$ is the total energy from DFT calculations, $E_{\text{energy}}^{\text{ZPE}}$ is the zero-point energy, $\int C_p dT$ the enthalpic change with the temperature, and E_{sol} the solvation energy. For adsorbed species, the term $(E_{\text{energy}}^{\text{ZPE}} + \int C_p dT - TS)$ was obtained at 298.15 K and computed within the harmonic limit employing the thermochemistry module available in the atomistic simulation environment package that uses the following equations:⁷

$$E_{\text{energy}}^{\text{ZPE}} = \sum_l \frac{1}{2} \varepsilon_l, \quad (4)$$

$$\int C_p dT = \sum_l \frac{\varepsilon_l}{e^{\varepsilon_l/k_B T} - 1}, \quad (5)$$

$$S = k_B \sum_l \frac{\varepsilon_l}{k_B T (e^{\varepsilon_l/k_B T} - 1)} - \ln \left(1 - e^{-\varepsilon_l/k_B T} \right), \quad (6)$$

where ε_l are the energies associated with the vibrational frequencies, k_B the Boltzmann constant, and T the temperature. While for E_{sol} we used values tabulated in a previous study according to the chemical group of the species,⁸ Section 8.

Finally, the highest positive free energy value among all the steps was the potential-determining step (PDS). Then, we defined the computed limiting potential for late steps in the reaction pathway as related to identified PDS, which provides the lowest electrode potential that should be applied to obtain a specific product via that reaction pathway:

$$U_{\text{PDS}} = -\frac{\Delta G_{\text{MAX}}}{e}. \quad (7)$$

6 Gas-phase Molecules within the CHE

The free energies for gas-phase molecules was obtained by:

$$G^g = E_{tot}^g + E_{energy}^{ZPE} + \int C_p dT - TS . \quad (8)$$

We calculated the E_{energy}^{ZPE} , $\int C_p dT$, and TS at 298.15 K and 101325 Pa within the ideal-gas limit as implemented in the thermochemistry module available in the atomistic simulation environment package.⁷ Table S11 provides the data obtained for gas-phase species of this study.

Table S11: Values of E_{energy}^{ZPE} , $\int C_p dT$, and TS for all gas-phase species involved in this study. All energetic quantities are given in eV.

Species	ZPE	$\int C_p dT$	TS
H ₂	0.27	0.00	0.42
H ₂ O	0.56	0.00	0.58
C ₂ H ₄	1.35	0.01	0.68
CH ₃ CHO	1.45	0.03	0.81
CH ₃ CH ₂ OH	2.10	0.04	0.84
CO	0.13	0.03	-0.61

7 Liquid-phase Corrections

We included the correction for liquid molecules like water and ethanol. Our liquid-phase correction uses the vapor pressure of the substance at which the liquid and gas phases are in equilibrium at 298.15 K, as employed by Nørskov et al.⁵ Then, we computed the TS term within the ideal-gas limit using those vapor pressures. Table S12 informs the vapor pressures employed and the TS terms obtained. It is common to employ a liquid-phase correction for acetaldehyde, but it is worth mentioning that at 298.15 K and 101325 Pa, the acetaldehyde would be in the gas phase. To be consistent with the conditions used to compute our data, we did not apply corrections for acetaldehyde. For complement, we included the data for this correction in Table S12, remaining the TS unaltered. It could be a consequence of the acetaldehyde's boiling point of 294.05 K, which implies slight changes (when compared to H₂O and CH₃CH₂OH) in the vapor pressure to keep the gas-liquid equilibrium.

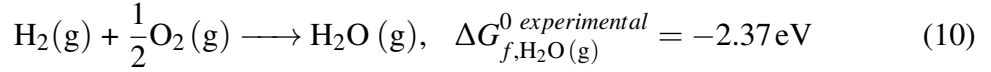
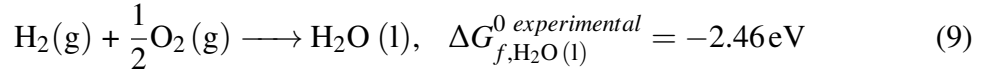
Table S12: Vapor pressures at which liquid and gas phases are in equilibrium at 298.15 K and TS term computed within the ideal-gas limit.

Molecule	vapor pressure (Pa)	TS (eV)
H ₂ O	3168 ⁹	0.67
CH ₃ CHO	120287 ¹⁰	0.81
CH ₃ CH ₂ OH	7906 ¹¹	0.91

We also inform an alternative liquid-phase correction widely employed by Calle-Vallejo.⁸

Below is the detailed procedure for H₂O:

1. Obtain the experimental standard Gibbs free energy of formation for the species in the gas and liquid phase at 298 K and 101325 Pa.¹²



2. Perform the difference between $\Delta G_{f,H_2O(l)}^{0 \text{ experimental}}$ and $\Delta G_{f,H_2O(g)}^{0 \text{ experimental}}$.

$$\Delta G_{f,H_2O(l)}^{0 \text{ experimental}} - \Delta G_{f,H_2O(g)}^{0 \text{ experimental}} = -0.09 \text{ eV} \quad (11)$$

equivalent to:

$$G_{H_2O}^l - G_{H_2O}^g = -0.09 \text{ eV} \quad (12)$$

3. Solve to get $G_{H_2O}^l$ and use the $G_{H_2O}^g$ coming from DFT calculations, equation (8).

$$\begin{aligned} G_{H_2O}^l &= E_{tot} + E_{energy}^{ZPE} + \int C_p dT - TS - 0.09 \\ &= E_{tot} + E_{energy}^{ZPE} + \int C_p dT - (TS + 0.09) \end{aligned} \quad (13)$$

Analogously for ethanol and acetaldehyde, the equation (12) becomes equations (14) and (15), respectively:

$$G_{CH_3CH_2OH}^l - G_{CH_3CH_2OH}^g = -0.07 \quad (14)$$

$$G_{CH_3CHO}^l - G_{CH_3CHO}^g = 0.06 \quad (15)$$

Then, solving those equations as in the equation (13):

$$\begin{aligned} G_{\text{CH}_3\text{CH}_2\text{OH}}^l &= E_{\text{tot}} + E_{\text{energy}}^{\text{ZPE}} + \int C_p dT - TS - 0.07 \\ &= E_{\text{tot}} + E_{\text{energy}}^{\text{ZPE}} + \int C_p dT - (TS + 0.07) \end{aligned} \quad (16)$$

$$\begin{aligned} G_{\text{CH}_3\text{CHO}}^l &= E_{\text{tot}} + E_{\text{energy}}^{\text{ZPE}} + \int C_p dT - TS + 0.06 \\ &= E_{\text{tot}} + E_{\text{energy}}^{\text{ZPE}} + \int C_p dT - (TS - 0.06) \end{aligned} \quad (17)$$

Table S13 informs the Gibbs free energies of formation employed and the value of the correction when included in the TS term.

Table S13: Experimental Gibbs free energies of formation¹² for Liquid-phase corrections and the TS corrected. All quantities are given in eV.

Molecule	$\Delta G_{f,(l)}^0$	$\Delta G_{f,(g)}^0$	$\Delta G_{f,(l)}^0 - \Delta G_{f,(g)}^0$	TS corrected
H ₂ O	-2.46	-2.37	-0.09	0.67
CH ₃ CHO	-1.32	-1.38	0.06	0.75
CH ₃ CH ₂ OH	-1.81	-1.74	-0.07	0.91

8 Solvation Contributions to the Free Energies

To consider the solvation contributions (E_{sol}) to free energy of the adsorbed systems (*), we employed an approach proposed in previous studies based on the functional groups of the species.^{8,13} Table S14 summarize the values according to the species type.

Table S14: Solvation contributions (E_{sol}) according to the functional group of the chemical species.¹³

Functional Group	E_{sol} (eV)
RCO*	-0.10
OH*	-0.50
ROH*	-0.38
OR*	-0.25

9 Free Energy Diagrams from CHCO to Ethanol and Ethylene

Below are data employed to build the free energy diagrams. We used as reference the Gibbs free energy of the adsorbed CHCO, $G^{\text{CHCO}*}$.

Table S15: Values employed of zero-point energy ($E_{\text{energy}}^{\text{ZPE}}$), entropic contribution (TS), enthalpic change with the temperature ($\int C_p dT$), solvation contribution (E_{sol}), and Gibbs free energy changes regarding to CHCO (ΔG) for all species considered in Figure S7 employing Cu₅₅ cluster. The * indicates adsorbed species on Cu₅₅.

Species	$E_{\text{energy}}^{\text{ZPE}}$	TS	$\int C_p dT$	E_{sol}	ΔG
CHCO*	0.60	0.24	0.11	-0.10	0.00
CHCOH*	0.90	0.18	0.10	-0.38	-0.22
CH ₂ CO*	0.87	0.34	0.13	-0.10	-0.11
CHCHO*	0.91	0.18	0.09	-0.25	-0.30
CH ₃ CO*	1.19	0.28	0.13	-0.10	-0.58
CH ₂ COH*	1.20	0.24	0.12	-0.38	-0.27
CHCH ₂ O*	1.21	0.31	0.12	-0.25	1.05
CHCHOH*	1.21	0.23	0.12	-0.38	-0.32
CH ₂ CHO*	1.21	0.21	0.11	-0.25	-0.80
C ₂ H ₄ (g) + O*	1.35 + 0.07	0.68 + 0.04	0.01 + 0.03	-	-0.25
CH ₃ CHO*	1.48	0.39	0.15	-0.25	-0.93
CH ₃ CHO(g)	1.45	0.81	0.03	-	-0.49
CH ₃ COH*	1.50	0.38	0.14	-0.38	-0.31
CH ₃ CH ₂ O*	1.80	0.28	0.14	-0.38	-1.05
CH ₃ CH ₂ OH (l)	2.10	0.91	0.04	-	-0.75
C ₂ H ₄ (g) + OH*	1.35 + 0.34	0.68 + 0.09	0.01 + 0.05	0.00 + (-0.50)	-1.11
C ₂ H ₄ (g) + H ₂ O (l)	1.35 + 0.56	0.68 + 0.67	0.01 + 0.00	-	-0.71

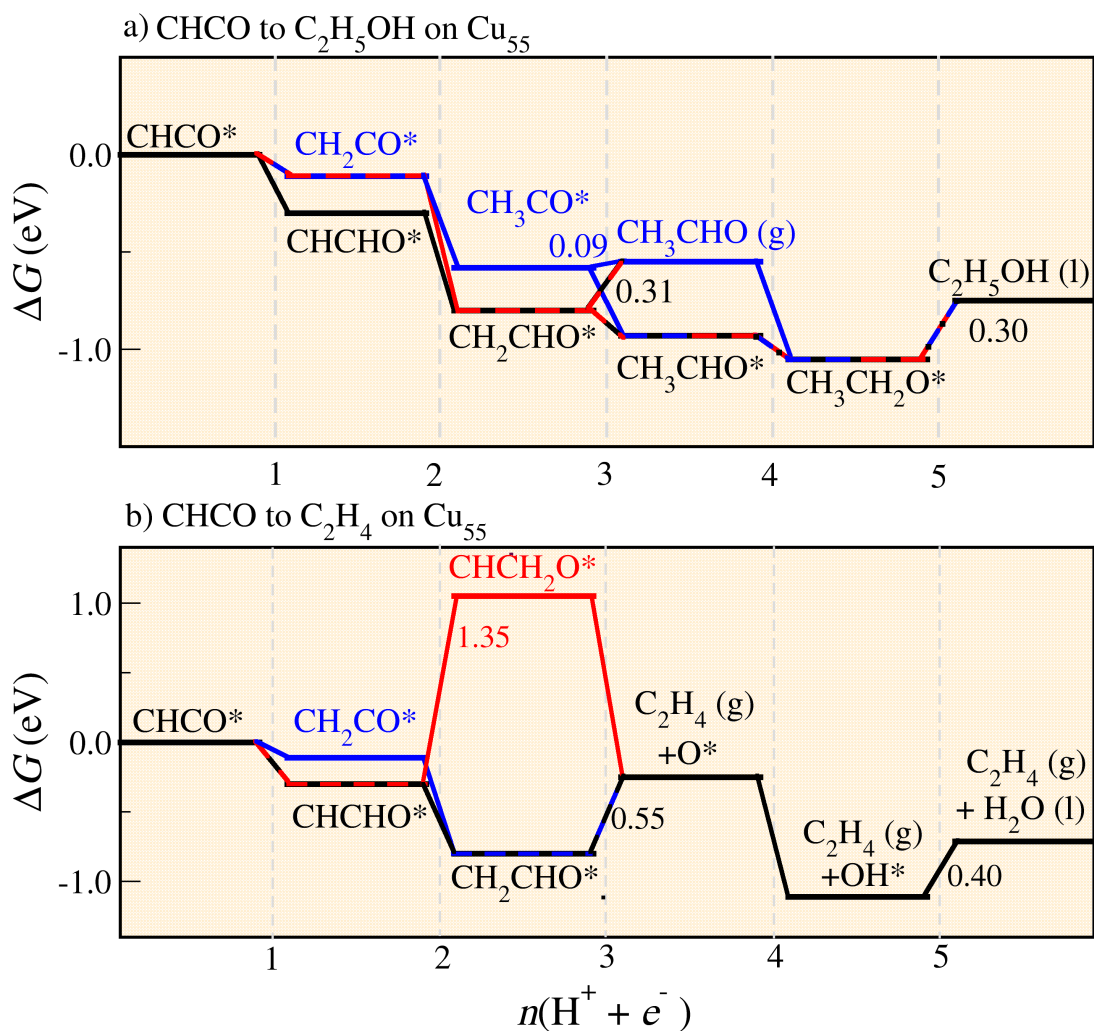


Figure S8: Free energy diagram from CHCO to a) $\text{CH}_3\text{CH}_2\text{OH}$ and b) C_2H_4 on Cu_{55} . The numbers are the values of ΔG in eV for the endergonic steps along the paths. Line in black connects the preferred reaction path, while red and blue lines correspond to other paths explored.

Table S16: Values employed of zero-point energy (E_{energy}^{ZPE}), entropic contribution (TS), enthalpic change with the temperature ($\int C_p dT$), solvation contribution (E_{sol}), and Gibbs free energy changes regarding to CHCO (ΔG) for all species considered in Figure S7 employing Cu₄₂Zn₁₃ cluster. The * indicates adsorbed species on Cu₄₂Zn₁₃.

Species	E_{energy}^{ZPE}	TS	$\int C_p dT$	E_{sol}	ΔG
CHCO*	0.61	0.24	0.11	-0.10	0.00
CHCOH*	0.92	0.19	0.10	-0.38	0.36
CH ₂ CO*	0.91	0.16	0.09	-0.10	0.17
CHCHO*	0.92	0.18	0.09	-0.25	-0.46
CH ₃ CO*	1.20	0.26	0.12	-0.10	-1.35
CH ₂ COH*	1.22	0.23	0.11	-0.38	0.03
CHCH ₂ O*	1.23	0.20	0.10	-0.25	1.08
CHCHOH*	1.22	0.26	0.12	-0.38	0.15
CH ₂ CHO*	1.21	0.24	0.12	-0.25	-0.91
C ₂ H ₄ (g) + O*	1.35 + 0.07	0.68 + 0.04	0.01 + 0.03	-	-0.11
CH ₃ CHO*	1.47	0.34	0.15	-0.25	-0.45
CH ₃ CHO(g)	1.45	0.81	0.03	-	-0.07
CH ₃ COH*	1.50	0.36	0.14	-0.38	0.10
CH ₃ CH ₂ O*	1.85	0.43	0.19	-0.38	-1.13
CH ₃ CH ₂ OH (l)	2.10	0.91	0.04	-	-0.32
C ₂ H ₄ (g) + OH*	1.35 + 0.35	0.68 + 0.10	0.01 + 0.05	0.00 + (-0.50)	-0.97
C ₂ H ₄ (g) + H ₂ O (l)	1.35 + 0.56	0.68 + 0.67	0.01 + 0.00	-	-0.29

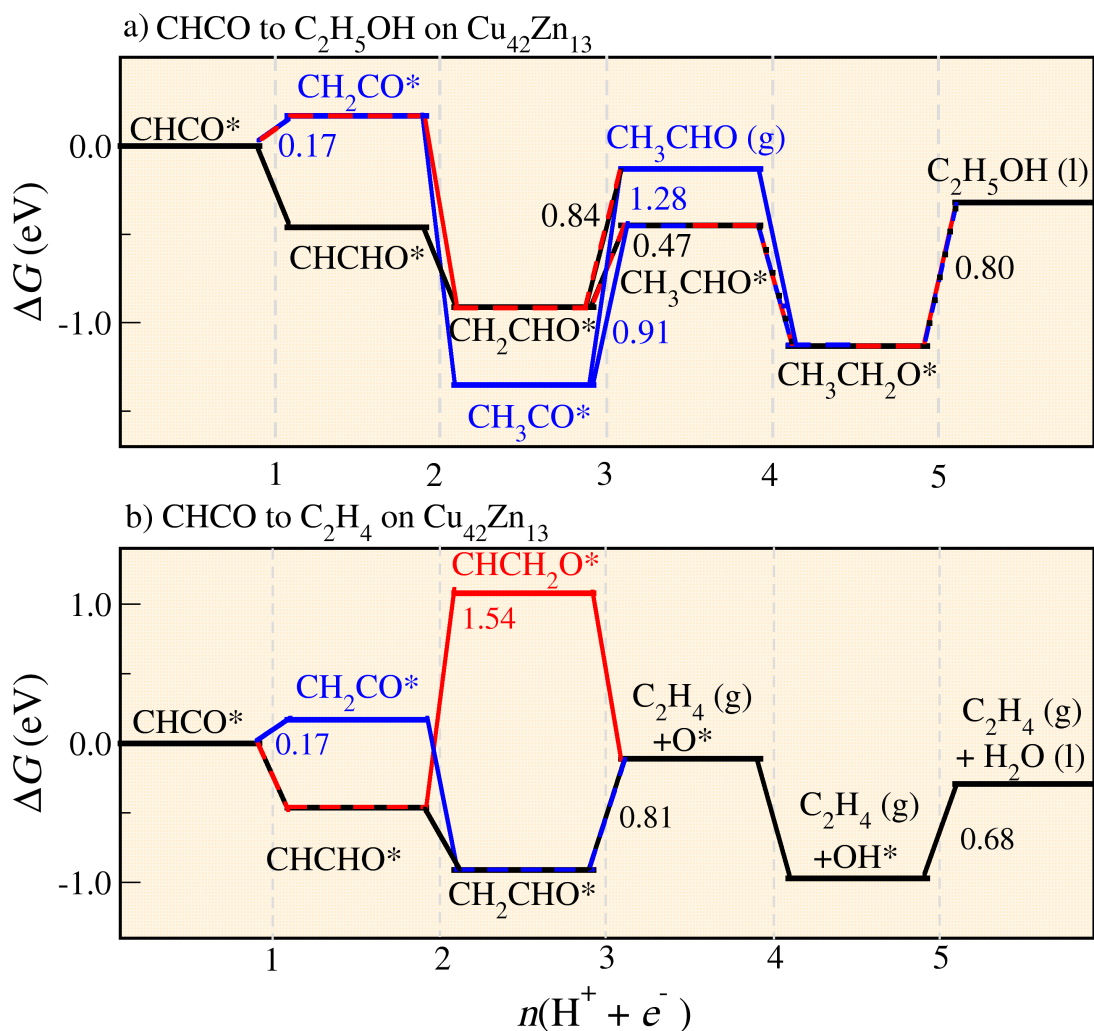


Figure S9: Free energy diagram from CHCO to a) $\text{CH}_3\text{CH}_2\text{OH}$ and b) C_2H_4 on $\text{Cu}_{42}\text{Zn}_{13}$. The numbers are the values of ΔG in eV for the endergonic steps along the paths. Line in black connects the preferred reaction path, while red and blue lines correspond to other paths explored.

10 Projected Density of States: Intermediates on Cu₅₅ and Cu₄₂Zn₁₃

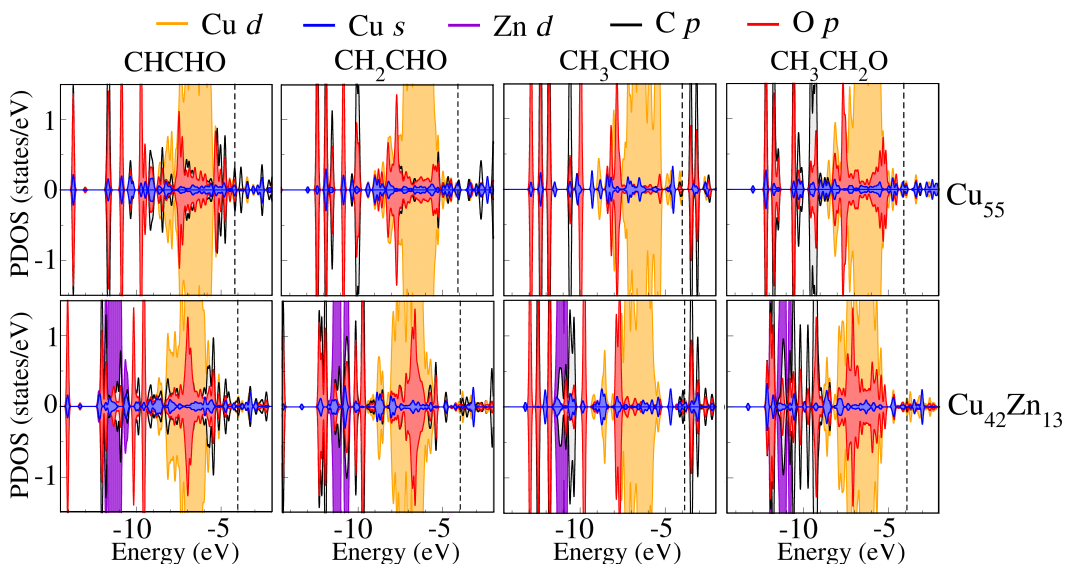


Figure S10: Projected density of states (PDOS) of C, O, and the TM atoms involved in the adsorption of the species on Cu₅₅ and Cu₄₂Zn₁₃ clusters.

References

- 1 Computational Chemistry Comparison and Benchmark DataBase (CCCBDB). 2015; <http://cccbdb.nist.gov/>.
- 2 Piotrowski, M. J.; Ungureanu, C. G.; Tereshchuk, P.; Batista, K. E. A.; Chaves, A. S.; Guedes-Sobrinho, D.; Da Silva, J. L. F. Theoretical Study of the Structural, Energetic, and Electronic Properties of 55-atom Metal Nanoclusters: A DFT Investigation Within van der Waals Corrections, Spin-Orbit Coupling, and PBE+U of 42 Metal Systems. *The Journal of Physical Chemistry C* **2016**, *120*, 28844–28856, DOI: 10.1021/acs.jpcc.6b10404.
- 3 Ye, W.; Guo, X.; Ma, T. A Review on Electrochemical Synthesized Copper-based Catalysts for Electrochemical Reduction of CO₂ to C₂+ Products. *J. Chem. Eng.* **2021**, *414*, 128825, DOI: 10.1016/j.cej.2021.128825.
- 4 da Silva, A. H.; Raaijman, S. J.; Santana, C. S.; Assaf, J. M.; Gomes, J. F.; Koper, M. T. Electrocatalytic CO₂ Reduction to C₂+ Products on Cu and CuxZny Electrodes: Effects of

Chemical Composition and Surface Morphology. *Journal of Electroanalytical Chemistry* **2021**, 880, 114750, DOI: 10.1016/j.jelechem.2020.114750.

- 5 Nørskov, J. K.; Rossmeisl, J.; Logadottir, A.; Lindqvist, L.; Kitchin, J. R.; Bligaard, T.; Jónsson, H. Origin of the Overpotential for Oxygen Reduction at a Fuel-Cell Cathode. *J. Phys. Chem. B* **2004**, 108, 17886–17892.
- 6 Peterson, A. A.; Abild-Pedersen, F.; Studt, F.; Rossmeisl, J.; Nørskov, J. K. How Copper Catalyzes the Electroreduction of Carbon Dioxide into Hydrocarbon Fuels. *Energy & Environmental Science* **2010**, 3, 1311, DOI: 10.1039/c0ee00071j.
- 7 Larsen, A. H.; Mortensen, J. J.; Blomqvist, J.; Castelli, I. E.; Christensen, R.; Dułak, M.; Friis, J.; Groves, M. N.; Hammer, B.; Hargus, C.; Hermes, E. D.; Jennings, P. C.; Jensen, P. B.; Kermode, J.; Kitchin, J. R.; Kolsbjerg, E. L.; Kubal, J.; Kaasbjerg, K.; Lysgaard, S.; Maronsson, J. B.; Maxson, T.; Olsen, T.; Pastewka, L.; Peterson, A.; Rostgaard, C.; Schiøtz, J.; Schütt, O.; Strange, M.; Thygesen, K. S.; Vegge, T.; Vilhelmsen, L.; Walter, M.; Zeng, Z.; Jacobsen, K. W. The atomic Simulation Environment—a Python Library for Working with Atoms. *J. Condens. Matter Phys.* **2017**, 29, 273002, DOI: 10.1088/1361-648x/aa680e.
- 8 Calle-Vallejo, F.; Koper, M. T. M. Theoretical Considerations on the Electroreduction of CO to C₂ Species on Cu(100) Electrodes. *Angewandte Chemie International Edition* **2013**, 52, 7282–7285, DOI: 10.1002/anie.201301470.
- 9 Lide, D. R., Ed. *CRC Handbook of Chemistry and Physics*; CRC Press: Boca Raton, 2005.
- 10 Boublík, T.; Fried, V.; Hála, E. *The Vapour Pressures of Pure Substances*; Elsevier Science Pub. Co., Inc., New York, NY, 1984.
- 11 Daubert, T. E. *Physical and Thermodynamic Properties of Pure Chemicals: Data Compilation*; AIChE, 1989.
- 12 Haynes, W. M. *CRC Handbook of Chemistry and Physics*, 95th ed.; CRC Press: Boca Raton, FL, USA, 2014.

13 Ting, L. R. L.; Piqué, O.; Lim, S. Y.; Tanhaei, M.; Calle-Vallejo, F.; Yeo, B. S. Enhancing CO₂ Electroreduction to Ethanol on Copper–Silver Composites by Opening an Alternative Catalytic Pathway. *ACS Catal.* **2020**, *10*, 4059–4069, DOI: 10.1021/acscad.9b05319.